SI Appendix, Matsui et al.

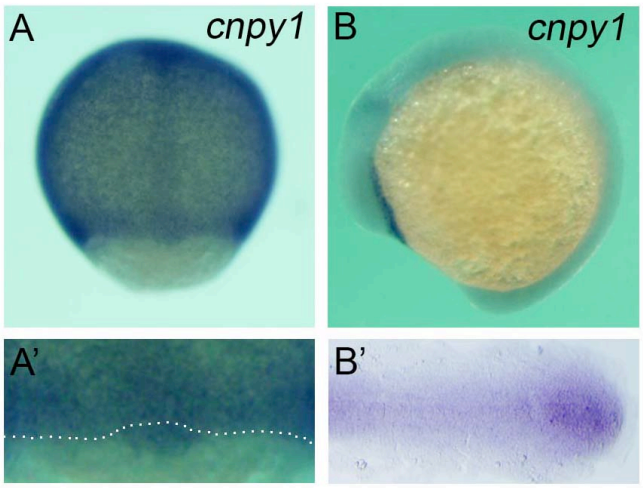

Figure S1. Expression of *cnpy1* in zebrafish early embryos. (A, B) Expression of *cnpy1* in embryos at 80% epiboly (A), or at the 6-somite stage (B). (A) Dorsal view, anterior to the top. (A') Higher-magnification image highlights DFCs. The white dotted line marks the boundary between DFCs and the blastoderm margin. (B) Lateral view, anterior to the left. (B') Flat-mounted embryo at the 6-somite stage. Dorsal view, anterior to the left. *cnpy1* expression at the 6-somite stage is restricted to the polster, MHB and tailbud.

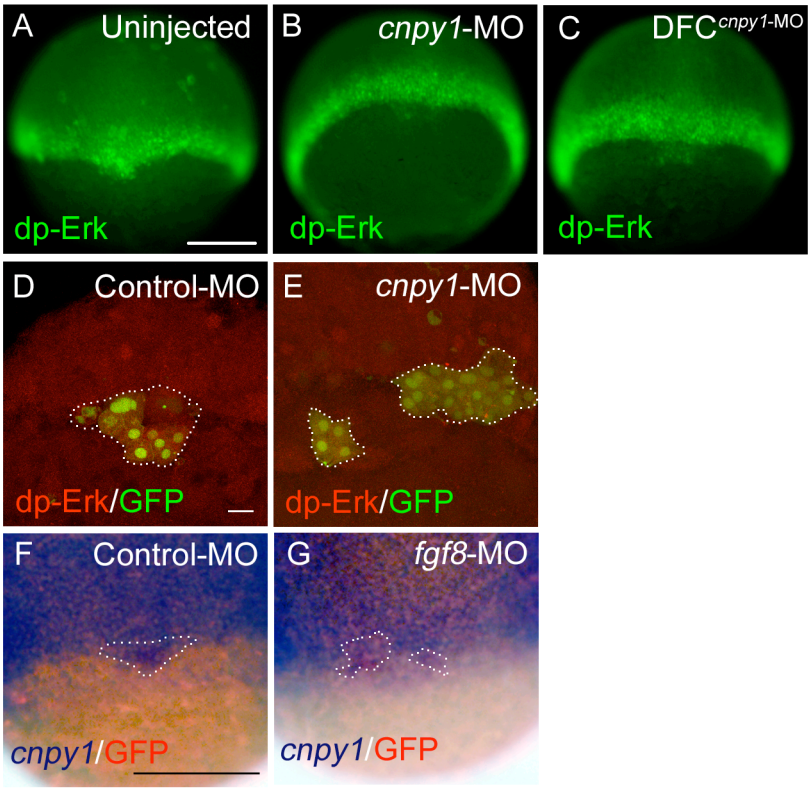

Figure S2. A positive control loop between Cnpy1 and FGF signaling is established in DFCs. (A-C) dp-Erk staining in uninjected (A), *cnpy1*-MO-injected (B) or DFC$^{cnpy1\text{-MO}}$-injected (C) embryos at 60% epiboly stage. Scale bar: 200 μm. (D, E) dp-Erk staining in control-MO-injected (D) or *cnpy1*-MO-injected (E) *Tg[sox17:GFP]* embryos at 60% epiboly stage. Scale bar: 20 μm. dp-Erk signals (red) were down-regulated in GFP-positive DFCs (green). (F, G) *cnpy1* (purple) and GFP (red) expression in control-MO-injected (F) or *fgf8*-MO-injected (G) *Tg[sox17:GFP]* embryos at 60% epiboly stage. Scale bar: 200 μm. Dotted lines mark the outlines of DFC populations.

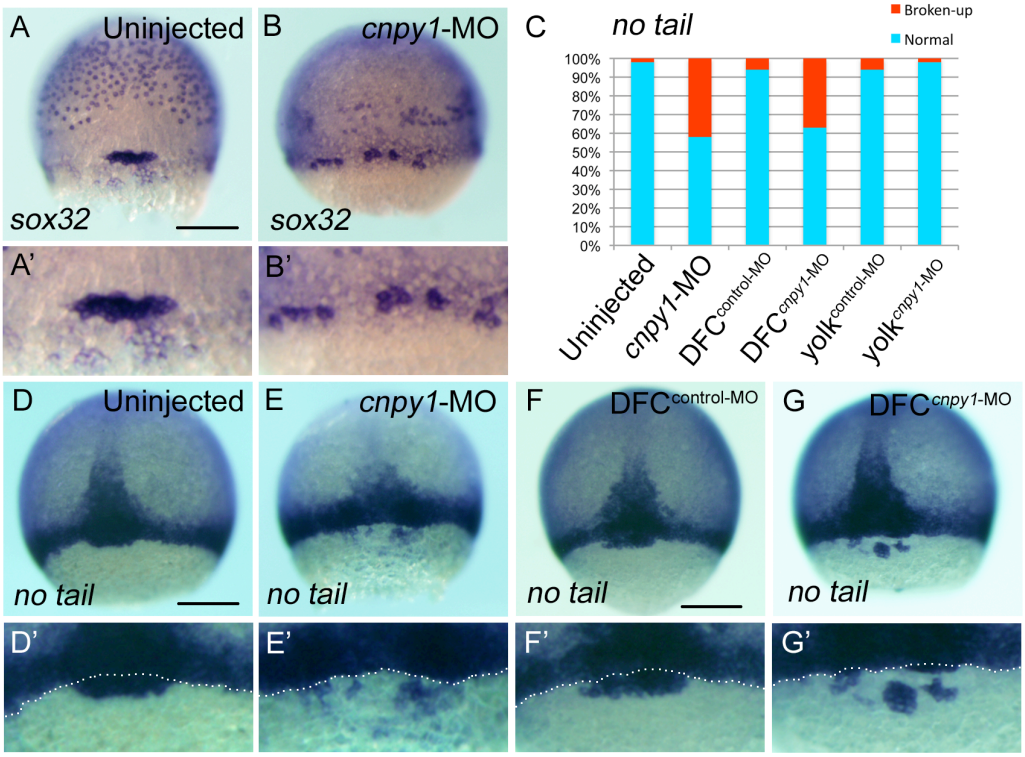

Figure S3. *cnpy1* function is essential for DFC clustering. (A, B) *sox32* expression in uninjected (A) or *cnpy1*-MO-injected (B) embryos. Scale bar: 200 µm. (C) Percentages of normal or broken-up DFCs were scored using the *no tail* expression pattern in uninjected (n = 84), *cnpy1*-MO (n = 55), DFC$^{\text{control-MO}}$ (n = 64), DFC$^{\textit{cnpy1}\text{-MO}}$ (n = 48), yolk$^{\text{control-MO}}$ (n = 50) or yolk$^{\textit{cnpy1}\text{-MO}}$ (n = 66) embryos. Statistically significant ($P < 0.05$) differences could be seen in uninjected versus *cnpy1*-MO ($P = 2.76 \times 10^{-9}$) and DFC$^{\text{control-MO}}$ versus DFC$^{\textit{cnpy1}\text{-MO}}$ ($P = 6.1 \times 10^{-5}$), while no difference was seen in uninjected versus DFC$^{\text{control-MO}}$ ($P = 0.403$), uninjected versus yolk$^{\text{control-MO}}$ ($P = 0.361$), DFC$^{\text{control-MO}}$ versus yolk$^{\text{control-MO}}$ ($P = 1.000$) or yolk$^{\text{control-MO}}$ versus yolk$^{\textit{cnpy1}\text{-MO}}$ ($P = 0.314$). (D-G) *no tail* expression in uninjected (D), *cnpy1*-MO-injected (E), DFC$^{\text{control-MO}}$ (F) or DFC$^{\textit{cnpy1}\text{-MO}}$ (G) embryos. Dorsal view, anterior to the top. Scale bar: 200 µm. (A'-D') Higher-magnification images highlight DFCs. The white dotted lines mark the boundary between DFCs and the blastoderm margin.

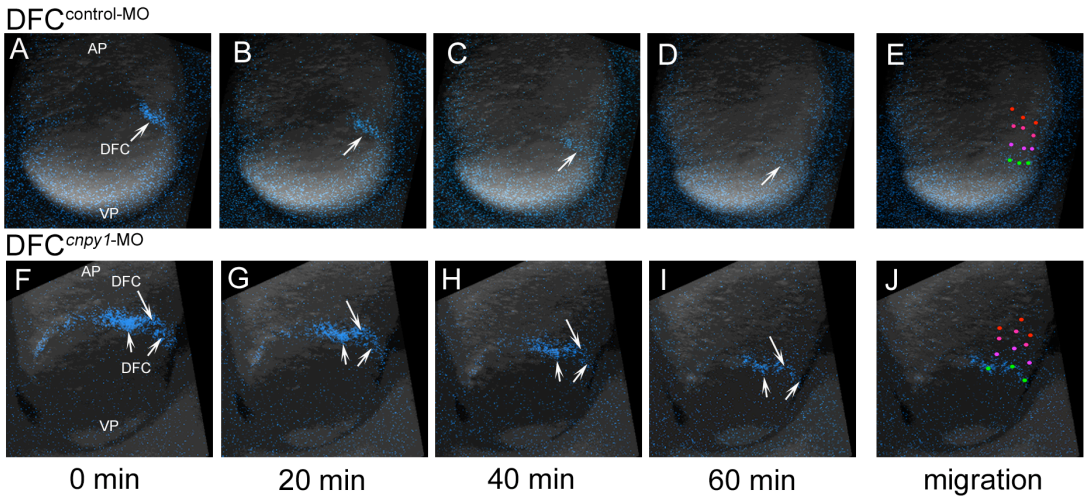

Figure S4. DFC-specific knockdown of *cnpy1* does not affect DFC migration towards the vegetal pole. (A-J) Time-lapse confocal imaging of DFC migration in DFC$^{\text{control-MO}}$-injected (A-E) or DFC$^{cnpy1\text{-MO}}$-injected (F-J) embryos. DFCs were labeled with SYTO17 tracer, and DFC migration was monitored every 2.5 min for 82.5 min. A, F; 0 min, B, G; 20 min, C, H; 40 min, D, I; 60 min. Although a DFC cluster (arrow in A) is found in the DFC$^{\text{control-MO}}$ embryo at 0 min, sparse DFC populations (arrows in F) appear in the DFC$^{cnpy1\text{-MO}}$ embryo. AP, animal pole; VP, vegetal pole. (E, J) Three cells in each embryo at 0 min are marked by red dots, and their migration is traced at 20-min intervals (indicated by color changes from red [0 min] to green [60 min]).

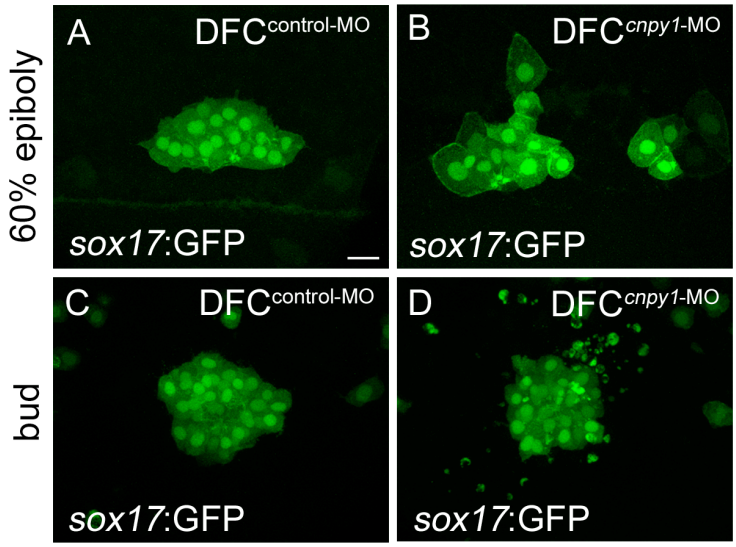

E DFC number

MO \ Stage	60% epiboly	bud
DFC$^{control\text{-}MO}$	22.9 ± 4.1 (n = 10)	33.9 ± 8.5 (n =16)
DFC$^{cnpy1\text{-}MO}$	23.0 ± 5.7 (n = 10)	23.4 ± 8.4 (n = 14)

Figure S5. The broken-up DFC phenotype in DFC$^{cnpy1\text{-}MO}$ embryos may interfere with proper recruitment of DFCs to the KV. (A-D) DFC morphology in *Tg[sox17:GFP]* embryos injected with control-MO (A, C; DFC$^{control\text{-}MO}$) or *cnpy1*-MO (B, D; DFC$^{cnpy1\text{-}MO}$). (A, B) Dorsal view of the embryos at 60% epiboly stage. (C, D) Vegetal pole view of the embryos at bud stage. Scale bar: 20 μm. (E) Number of DFCs scored by GFP expression.

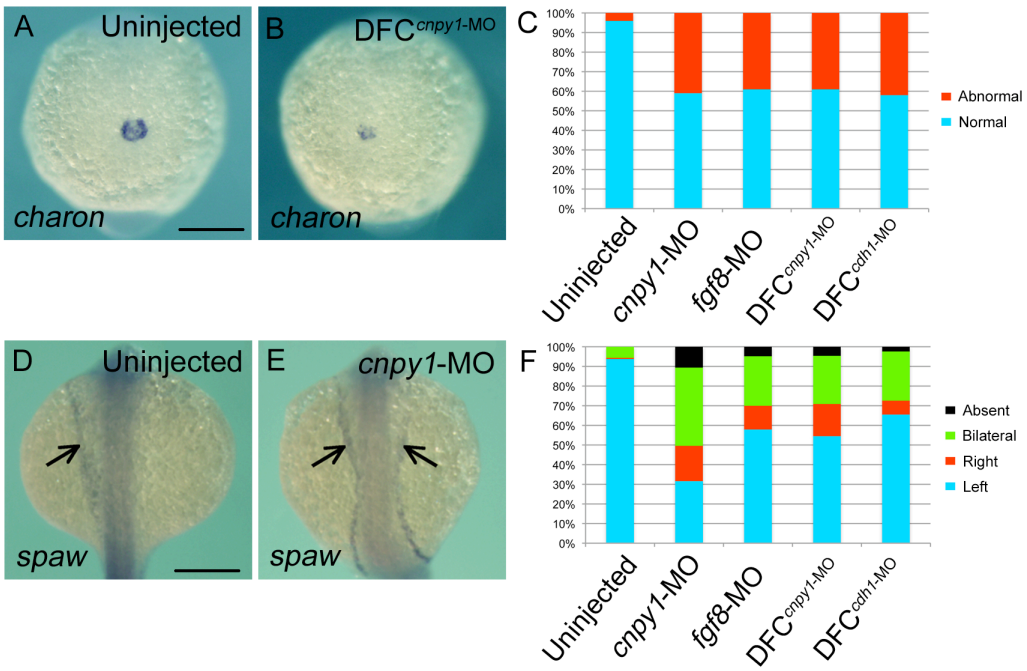

Figure S6. Loss of FGF signaling leads to defects in KV formation and LR patterning. (A, B) Representative images showing horseshoe-shaped (uninjected; A) or abnormal (DFC$^{cnpy1\text{-MO}}$; B) patterns of *charon* expression in embryos at the 6-somite stage. Vegetal pole view. Scale bar: 200 μm. (C) Percentages of normal or abnormal phenotypes were scored using the *charon* expression pattern in uninjected (n = 54), *cnpy1*-MO (n = 73), *fgf8*-MO (n = 66), DFC$^{cnpy1\text{-MO}}$ (n = 72) or DFC$^{cdh1\text{-MO}}$ (n = 71) embryos. Statistically significant ($P < 0.05$) differences could be seen in uninjected versus *cnpy1*-MO ($P = 5.66 \times 10^{-8}$), *fgf8*-MO ($P = 4.99 \times 10^{-7}$), DFC$^{cnpy1\text{-MO}}$ ($P = 4.14 \times 10^{-7}$) and DFC$^{cdh1\text{-MO}}$ ($P = 6.40 \times 10^{-8}$). (D, E) Representative images demonstrating left-sided (uninjected; D) or bilateral (*cnpy1*-MO; E) expression of *spaw* at the 20-somite stege. Dorsal view, anterior to the top. Scale bar: 200 μm. (F) Percentage of left-sided, right-sided, bilateral, or no (absent) expression of *spaw* in uninjected (n = 156), *cnpy1*-MO (n = 133), *fgf8*-MO (n = 108), DFC$^{cnpy1\text{-MO}}$ (n = 110) or DFC$^{cdh1\text{-MO}}$ (n = 84) embryos. Statistically significant ($P < 0.05$) differences could be seen in uninjected versus *cnpy1*-MO ($P < 2.2 \times 10^{-16}$), *fgf8*-MO ($P = 4.96 \times 10^{-16}$), DFC$^{cnpy1\text{-MO}}$ ($P < 2.2 \times 10^{-16}$) and DFC$^{cdh1\text{-MO}}$ ($P = 9.21 \times 10^{-11}$).

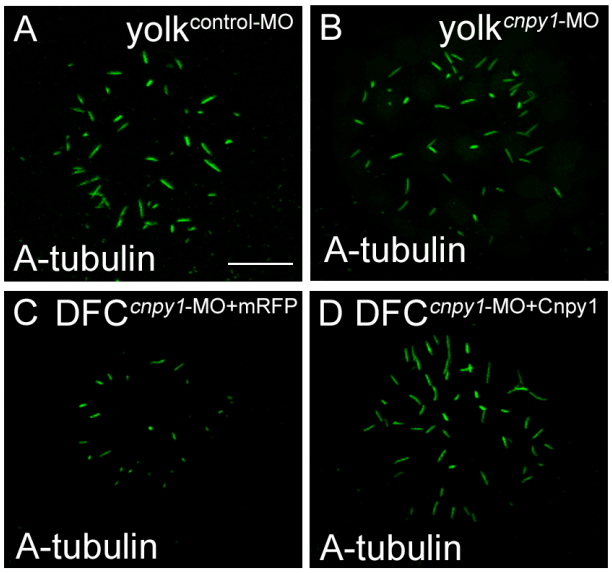

Figure S7. Cnpy1 function in DFCs is required for ciliogenesis in the KV. (A-D) A-tubulin staining in yolk$^{\text{control-MO}}$ (A), yolk$^{cnpy1\text{-MO}}$ (B), DFC$^{cnpy1\text{-MO+mRFP}}$ (C) and DFC$^{cnpy1\text{-MO+Cnpy1}}$ (D) embryos at the 6-somite stage. Vegetal pole view. Scale bar: 20 μm.

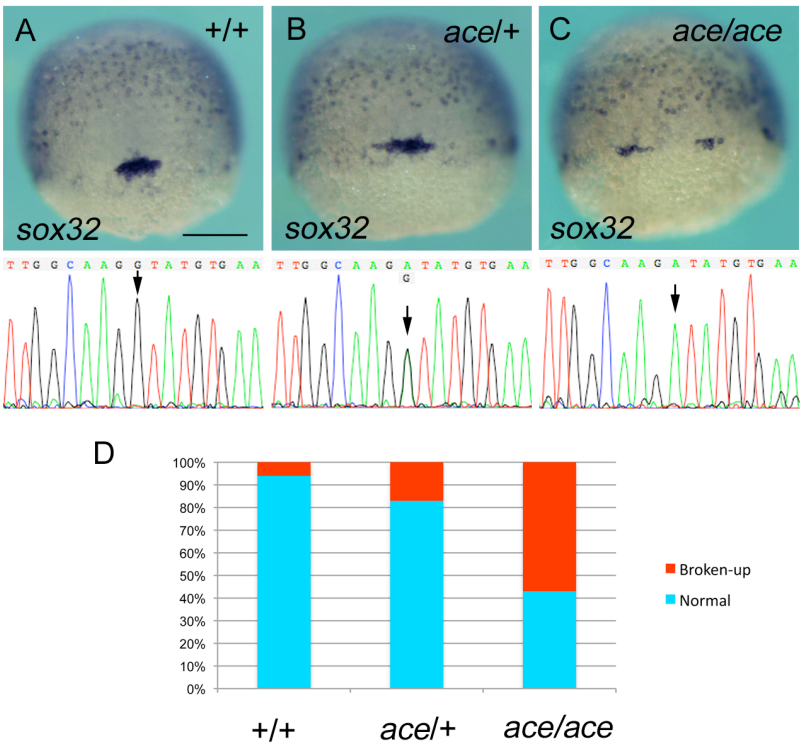

Figure S8. *ace/fgf8* mutants result in the broken-up DFC phenotype. (A-C) Upper panels indicate *sox32* expression in wild type (+/+; A), *ace* heterozygote (*ace*/+; B), *ace* homozygote (*ace/ace*; C) at 70% epiboly. Scale bar: 200 μm. Lower panels show sequences around the *ace* mutation. Arrows indicate the position of the *ace* mutation. Substitution from G to A occurs in the *ace* allele. (D) Percentages of normal or broken-up DFCs were scored using the *sox32* expression pattern in wild type (n = 17), *ace* heterozygote (n = 36) or *ace* homozygote (n = 14).

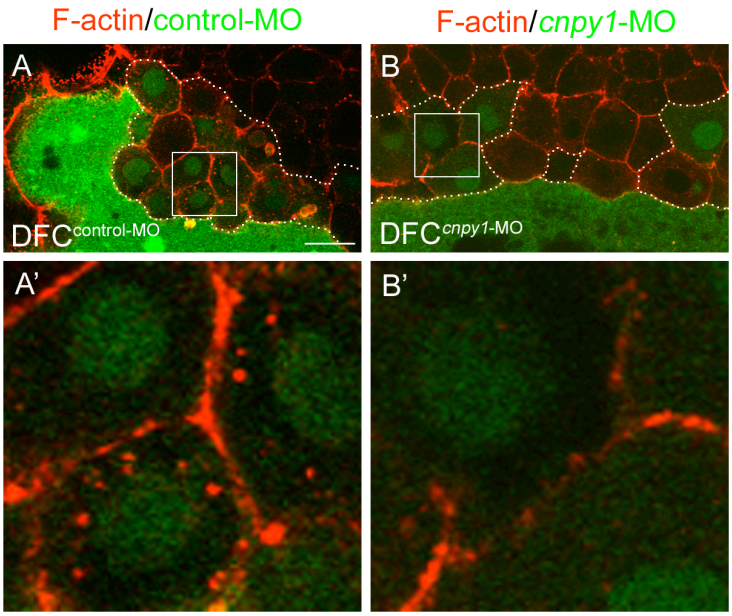

Figure S9. DFC-specific knockdown of *cnpy1* attenuates F-actin accumulation at the cell-cell contact sites of DFCs. (A, B) Distribution of F-actin (red) and FITC-labeled MO (green) in DFC$^{\text{control-MO}}$ (A) or DFC$^{\textit{cnpy1}\text{-MO}}$ (B) embryos. Dorsal view, anterior to the top. Scale bar: 20 μm. White dotted lines mark the plasma membrane outlines of MO-containing DFC populations. (A', B') Higher-magnification images highlight MO-containing DFCs. In control-MO-containing DFCs (A'), F-actin accumulated at the cell-cell contact sites of the plasma membrane. However, accumulation of F-actin was limited in *cnpy1*-MO-containing DFCs (B').

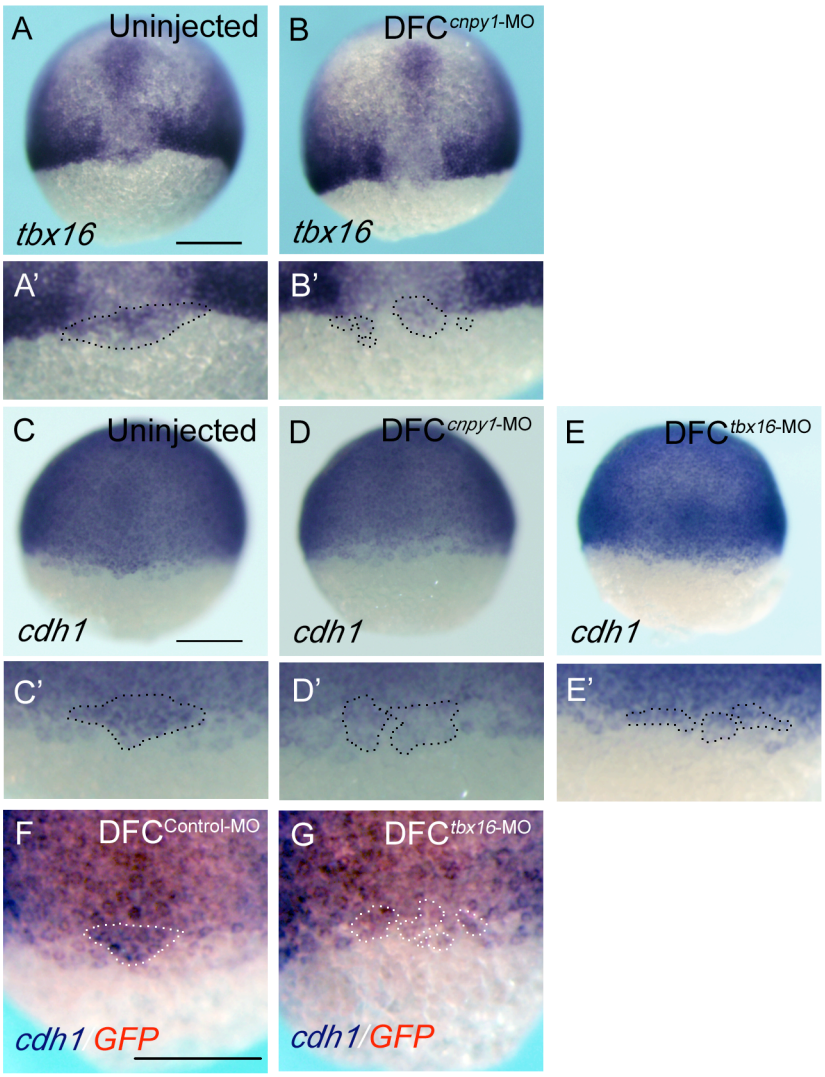

Figure S10. A genetic cascade including *tbx16* and *cdh1* mediates FGF signaling in DFCs. (A, B) Dorsal view of *tbx16* expression in uninjected (A) or DFC$^{cnpy1\text{-MO}}$ (B) embryos at 65% epiboly stage. Scale bar: 200 μm. (C-E) Dorsal view of *cdh1* expression in uninjected (C), DFC$^{cnpy1\text{-MO}}$-injected (D) or DFC$^{tbx16\text{-MO}}$-injected (E) embryos at 65% epiboly stage. Scale bar: 200 μm. (A'-E') Higher-magnification images highlight DFCs. (F, G) *cdh1* (purple) and GFP (red) expression in DFC$^{control\text{-MO}}$-injected (F) or DFC$^{tbx16\text{-MO}}$-injected (G) *Tg[sox17:GFP]* embryos at 60% epiboly stage. Scale bar: 200 μm. Dotted lines in panels A'-E', F and G mark the outlines of the DFC populations.

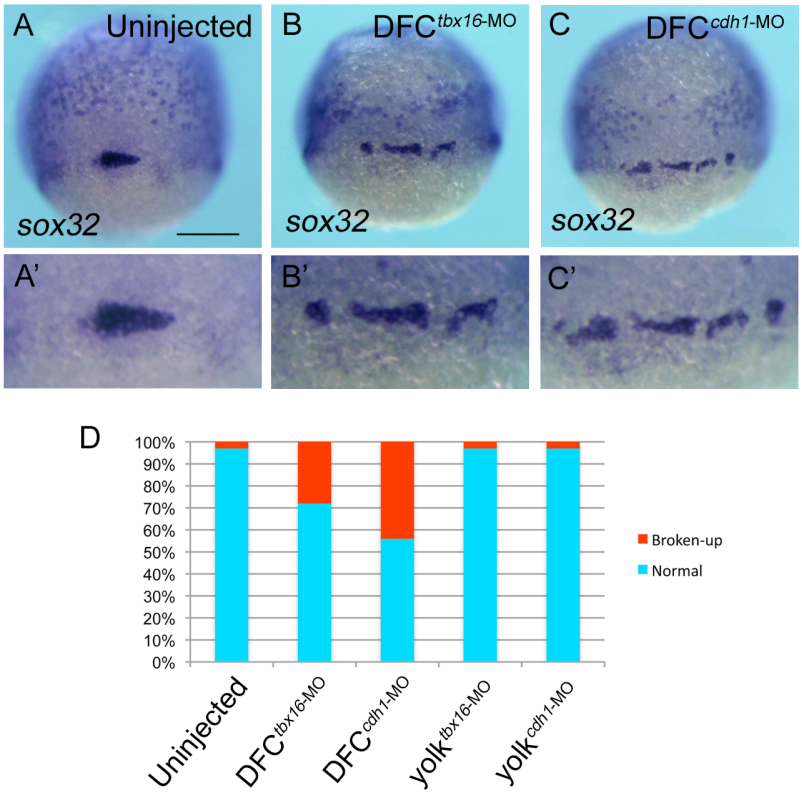

Figure S11. DFC-specific knockdown of *tbx16* or *cdh1* results in the broken-up DFC phenotype. (A-C) Dorsal view of *sox32* expression in uninjected (A), DFC$^{tbx16\text{-MO}}$ (B) or DFC$^{chd1\text{-MO}}$ (C) embryos at 65% epiboly stage. Dorsal view, anterior to the top. Scale bar: 200 μm. (D) Percentages of normal or broken-up DFCs were scored using the *sox32* expression pattern in uninjected (n = 64), DFC$^{tbx16\text{-MO}}$ (n = 55), DFC$^{cdh1\text{-MO}}$ (n = 69) yolk$^{tbx16\text{-MO}}$ (n = 61) and yolk$^{cdh1\text{-MO}}$ (n = 65) embryos. Statistically significant ($P < 0.05$) differences could be seen in uninjected versus DFC$^{tbx16\text{-MO}}$ ($P = 1.68 \times 10^{-4}$) and DFC$^{cdh1\text{-MO}}$ ($P = 1.17 \times 10^{-8}$), but not between uninjected and yolk$^{tbx16\text{-MO}}$ ($P = 1.00$) or yolk$^{cdh1\text{-MO}}$ ($P = 1.00$).

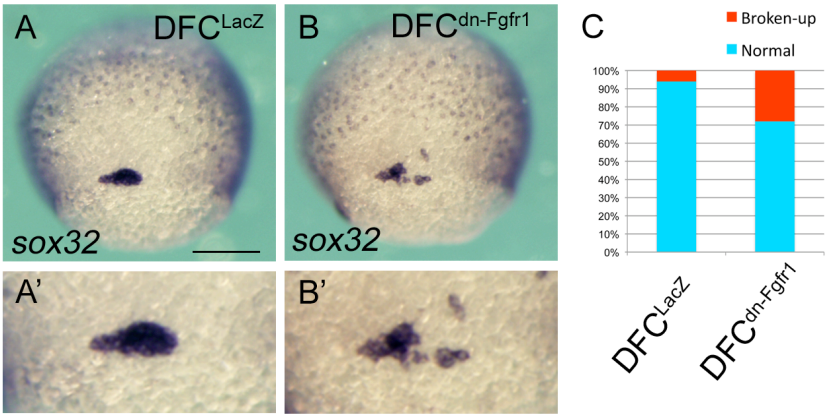

Figure S12. DFC-specific overexpression of dn-Fgfr1 can lead to broken-up DFC clusters. (A, B) Dorsal view of *sox32* expression of DFC^{LacZ}-injected (A) or $DFC^{dn\text{-}Fgfr1}$-injected (B) embryos. Scale bar: 200 μm. (C) Percentages of normal or broken-up DFCs were scored using the *sox32* expression pattern in DFC^{LacZ}-injected (n = 54) or $DFC^{dn\text{-}Fgfr1}$-injected (n = 47) embryos. A significant difference (P = 0.0025) could be seen between DFC^{LacZ} and $DFC^{dn\text{-}Fgfr1}$.

Table S1

Number of DFCs in loss-of-function embryos of FGF signaling

MO	Total number of DFCs	Number of embryos
Uninjected	22.5 ± 2.8	21
cnpy1-MO	21.3 ± 2.8	24
fgf8-MO	21.7 ± 5.0	20
DFC$^{\text{control-MO}}$	22.5 ± 2.3	27
DFC$^{\textit{cnpy1}\text{-MO}}$	22.1 ± 2.7	22
DFC$^{\textit{tbx16}\text{-MO}}$	21.2 ± 3.1	22
DFC$^{\textit{cdh1}\text{-MO}}$	20.1 ± 2.9	19
yolk$^{\text{control-MO}}$	22.3 ± 2.8	19
yolk$^{\textit{cnpy1}\text{-MO}}$	21.9 ± 3.9	18

Table S2

hCnpy2-interacting proteins identified by LC-MS/MS analysis				
Protein identified	Length	M.W. (kDa)	ER retention	Function
UGGT	1531	177.8	REEL	ER chaperones and folding-assisting enzymes
ORP150	999	111.4	NDEL	
GANAB	963	109.8	-	
GRP94	803	92.6	KDEL	
Calnexin	592	68.0	-	
BiP/GRP78	654	72.4	KDEL	
PDIA4	645	73.2	KEEL	
PDIA6	406	48.5	RDEL	
ERp46	432	48.2	KDEL	

UGGT: UDP-glucose ceramide glucosyltransferase-like 1; ORP150: 150-kDa oxygen-regulated protein; GANAB: neutral alpha-glucosidase AB; GRP94: 94-kDa glucose-regulated protein; PDIA4/6: protein disulfide-isomerase A4/6; ERp46: 46-kDa endoplasmic reticulum protein.

Movie Legends

Movie S1

This movie shows the dorsal-lateral view of a DFC$^{\text{control-MO}}$ embryo labeled with SYTO17 to reveal DFC migration. The time lapse covers a period of about 80 min, during the epiboly stages. By following cells during the course of the movie, we confirmed that the DFC cluster migrates downward during epiboly movements. (QuickTime 3.4 MB)

Movie S2

This movie shows the dorsal-lateral view of a DFC$^{\textit{cnpy1}\text{-MO}}$ embryo labeled with SYTO17 to reveal DFC migration. The time lapse covers a period of about 80 min. By following cells during the course of the movie, we observed that small DFC populations never assembled although downward migration occurred normally. (QuickTime 2.3 MB)

Materials and Methods

Morpholinos and injection

Non-labeled and FITC-labeled antisense MO oligonucleotides were obtained from Gene Tools. MOs against *fgf8*, *cnpy1, cdh1,* or a control MO, were used in this study. The sequences of MOs were as follows:

control-MO: 5'-CCTCTTACCTCAGTTACAATTTATA-3';

cnpy1-MO: 5'-ATGGTGACATGCTGGTCTCCTGAG-3'(1);

fgf8-MO: 5'-GAGTCTCATGTTTATAGCCTCAGTA-3' (2, 3);

tbx16-MO: 5'-GCTTGAGGTCTCTGATAGCCTGCAT-3' (4, 5);

cdh1-MO: 5'-AAGCATTTCTCACCTCTCTGTCCAG-3' (6, 7).

The efficacy of *cnpy1*-MO in inhibiting *cnpy1* translation was tested *in vivo* as we described before (1). The efficacy of *fgf8*-MO and *cdh1*-MO was confirmed *in vivo* by their ability to phenocopy the *ace/fgf8, spade tail/ tbx16* or *half backed/cdh1* zebrafish mutants, as shown previously (2, 4, 6).

To knock down genes in the entire embryo, non-labeled or FITC-labeled MOs (2.5-5 ng) were injected into the yolk of one-cell-stage zebrafish embryos as described previously (8). In contrast, DFC cluster-specific MO delivery was performed by injection of FITC-labeled MOs (2.5-5 ng) into the yolk of embryos at the 256-512-cell stages, as described (5, 9, 10). Only embryos in which FITC-labeled MOs entered DFCs were selected and used in this study. As a control, FITC-labeled MOs were delivered into yolk alone by injection into the yolk of embryos at the dome stage (5, 10).

Injected embryos were collected and fixed at the indicated time points, and then used for experiments such as *in situ* hybridization and immunostaining. Each such experiment was repeated at least three times.

SU5402 treatment

Embryos were obtained by mating wild-type fish and were cultured normally until 6 hours postfertilization (hpf). Embryos were cultured in embryo medium containing 100 μg/ml SU5402 for 1 h. After washing, embryos were fixed and used for *in situ* hybridization.

Time-lapse confocal imaging

Embryos at the shield stage were stained with SYTO17 dye (Invitrogen) for 30 min, washed with embryo medium, and embedded in 1% low-melt agarose. Time-lapse image acquisition was performed with an Olympus FV-1000-D confocal microscope and FLUOVIEW software.

Immunofluorescence analyses and F-actin staining

Embryos were fixed with 4% PFA at 4 ^{o}C for 10-16 h and dehydrated with methanol. Re-hydrated embryos were treated with 1% Triton X-100, 6% H_2O_2 in PBS for 20 min, washed with MABDT (0.1 M maleic acid pH 7.5, 150 mM NaCl, 1% DMSO, 0.1% Triton X-100), and blocked with 2% FBS in MABDT for at least 1 h. The embryos were then incubated with mouse monoclonal antibodies against acetylated tubulin (1:400; Sigma) or dp-Erk (1:2000; Sigma) in MABDT at 4 ^{o}C for at least 24 h. To detect acetylated tubulin, the embryos were washed with MABDT and incubated with Alexa Fluor 488 goat anti-mouse IgG (1:250; Invitrogen) at room temperature (RT) for 4 h, washed with MABDT, and flat-mounted in VECTASHIELD mounting medium (Vector Laboratories). To detect phosphorylated Erk, the embryos were washed with MABDT and incubated with HRP goat anti-mouse IgG (1:100; Invitrogen) or Alexa Fluor 555 goat anti-mouse IgG (1:250; Invitrogen) at 4 ^{o}C for at least 12 h. After MABDT washing, the signals were detected and amplified using an Alexa Fluor 488-Tyramide Signal Amplification Kit following the manufacturer's instructions (Invitrogen). To detect F-actin, the embryos were fixed with 4% PFA for 10-16 h and washed with PBS. The embryos were treated with 1% Triton X-100 in PBS for 30 min, incubated with rhodamine-phalloidin (1:200, Invitrogen) for 30-60 min, and washed with PBS several times. Immunofluorescence signals were visualized and photographed using an SZX12 stereo microscope (Olympus), or LSM510-META or LSM-Duo confocal microscopes (Zeiss).

To visualize the location of GFP-positive DFCs after *in situ* hybridization, *Tg[sox17:GFP]* embryos were incubated with rat anti-GFP antibody (1:2000; Nacalai tesque) in MABDT at 4 ^{o}C for at least 24 h. The embryos were washed with MABDT and incubated with HRP donkey anti-rat IgG (1:2000; Jackson ImmunoResearch) at 4 ^{o}C for at least 12 h. After MABDT washing, the signals were detected by the NovaRED

substrate kit (Vector Laboratories) according to the manufacturer's protocol and photographed using an SZX12 stereo microscope (Olympus).

Statistics

Number and length of primary cilia in the KV were analyzed using Welch's *t*-test, and other phenotypes such as broken-up DFC clusters and laterality defects were evaluated by Fisher's exact test. Results were considered significant when $P < 0.05$. Results are expressed as mean +/- s.e.m.

***In vitro* glycosidase assay and immunoprecipitation**

Peptide-N-glycosidase F (PNGase F) and endoglycosidase H (endo H) (Sigma) were used according to the manufacturer's instructions in an *in vivo* glycosidase assay with mouse embryonic fibroblast NIH3T3 cells (see below, *Guiding principle1*).

pCS2-$fgfr1_{Ext\text{-}HA}$ vector was transfected into 50% confluent cells, with pCS2-$cnpy1_{3xFlag}$ or pCS2 vector as a control. After 48 h cultivation, the cells were lysed with lysis buffer (PBS containing 1% Triton X-100, 0.2% SDS, 1 mM $MgCl_2$, and 1 mM $CaCl_2$) and treated with the glycosidases. Cleaved and uncleaved proteins were visualized by western blotting using anti-HA probe (Y-11) antibody (1:2000; Santa Cruz). The ratio of glycosylated to non-glycosylated Fgfr1 was estimated by quantitative analysis using the Scion image program.

Guiding principle1: PNGase F cleaves nearly all types of N-linked glycoproteins, whereas endo H specifically cleaves high-mannose-type N-linked glycoproteins within the ER. From the differences in their sensitivity, we could estimate the ratio of mature to immature proteins. Thus, the sub-fraction of proteins which is PNGase F-sensitive and endo H-resistant represents the mature forms of proteins; the other sub-fraction, which is sensitive to both PNGase F and endo H, represents the immature forms of proteins within the ER.

Identification of proteins binding to human Cnpy1 homolog by LC-MS/MS analysis

Since a full-length cDNA of the human *Cnpy1* ortholog has not been identified, we used the human *Cnpy1* homolog h*Cnpy2* (1) in LC-MS/MS analysis. Human embryonic kidney 293T cells were transfected with pCS2-h$Cnpy2_{Flag}$ or with pCS2 vector as a

control. After 48 h cultivation, the cells were crosslinked with dithiobis (succinimidyl propionate) (DSP) (Thermo) and lysed with PBS containing 1% Triton X-100, 1 mM $MgCl_2$, and 1 mM $CaCl_2$. Affinity-purified proteins from the cells were separated by SDS-PAGE and stained by MS-compatible silver staining to identify hCnpy2-binding proteins. The protein bands were excised and subjected to in-gel trypsin digestion. The extracted tryptic peptides were concentrated by vacuum centrifugation and analyzed by LC-MS/MS.

LC-MS/MS analyses were performed on the Nanofrontier L system, consisting of a nano-flow HPLC and LIT-TOF mass spectrometer (Hitachi High-technologies). The acquired MS/MS spectra were used to search against the IPI human version 3.16 database using the Mascot 2.1 searching algorithm (Matrix Science).

Restoration of defects in DFC$^{cnpy1\text{-}MO}$ embryos by conditional activation of FGF signaling, or overexpression of Cdh1 or Cnpy1

pCS2-*iFGFR1* (see below, *Guiding principle2*), pCS2-mouse *Cadherin1* (*Cdh1*, a kind gift from Drs. M. Hibi and M. Takeichi), pCS2-MO-resistant *cnpy1* and pCS2-*monomeric red fluorescent protein* (*mRFP*) were used in this study (1, 12). *iFGFR1*, *Cdh1* and *mRFP* mRNA were synthesized using the SP6 mMessage mMachine System (Ambion).

cnpy1-MO (5 ng) and *iFGFR1* mRNA (2.5 pg) were co-injected into embryos at the 256- to 512-cell stages, and these embryos were allowed to grow until 6 hpf. They were then separated into two pools, one of which was incubated with AP20187 (0.5 mM) until 10 hpf and the other with the same concentrations of ethanol (vehicle) until 10 hpf. After extensive washing, each pool was incubated in embryo medium and then collected for analyses at the indicated time points.

cnpy1-MO (5 ng) and either *Cdh1* mRNA (50 pg) or *mRFP* mRNA (50 pg), or *cnpy1*-MO (5 ng) and either MO-resistant *cnpy1* mRNA(100 pg) or *mRFP* mRNA (100 pg), were co-injected into 256- to 512-cell-stage embryos, and the chimeric embryos were incubated until the indicated time points.

Guiding principle2: iFGFR1 is an inducible system which activates FGF signaling by conditional dimerization of modified Fgfr1 (1, 13). In the presence of AP20187

(ARIAD), iFGFR1 dimerizes and activates downstream signal pathways of Fgfr1. Because iFGFR1 possesses a myristoylation signal for tethering to the cell membrane, it can mature and function in the absence of Cnpy1.

Genotyping of *ace*^{ti282a} embryos at mid-gastrulation

In situ hybridization using a *sox32* probe was performed in embryos at mid-gastrulation, obtained by intercrossing *ace*/+ heterozygous zebrafish. Because we could not recognize *ace*/*ace* homozygous embryos by visual observation, we performed genotyping of embryos following *in situ* hybridization. A 572-bp DNA fragment was amplified from genomic DNA extracted from each embryo, using the following pair of primers: 5'-CCAAGCTTATAGTAGAGACGGACACATTTG-3' and 5'-GTGCCAAGCAGATGGTCCACCT-3'. As shown in Fig. S8, substitution from G to A in the *ace* allele was detected by sequence analyses of the DNA fragment obtained from each embryo.

Effects of Fgfr1 on DFC clustering

The pCS2-dominant negative form of human Fgfr1 (dn-Fgfr1, a kind gift from Dr. K. Sakaguchi), which lacks the cytoplasmic domain, and pCS2-LacZ were used in this study. *dn-Fgfr1* and *LacZ* mRNAs were synthesized using the SP6 mMessage mMachine System (Ambion). *dn-Fgfr1* mRNA(100 pg) or *LacZ* mRNA (100 pg) was injected into 256- to 512-cell-stage embryos, and the chimeric embryos were incubated until the indicated time points.

References

1. Hirate, Y. & Okamoto, H. Canopy1, a novel regulator of FGF signaling around the midbrain-hindbrain boundary in zebrafish. *Curr Biol* 16, 421-7 (2006).
2. Maroon, H. et al. Fgf3 and Fgf8 are required together for formation of the otic placode and vesicle. *Development* 129, 2099-108 (2002).
3. Kawakami, Y., Raya, A., Raya, R. M., Rodriguez-Esteban, C. & Belmonte, J. C. Retinoic acid signalling links left-right asymmetric patterning and bilaterally symmetric somitogenesis in the zebrafish embryo. *Nature* 435, 165-71 (2005).
4. Bisgrove, B. W., Snarr, B. S., Emrazian, A. & Yost, H. J. Polaris and Polycystin-2 in dorsal forerunner cells and Kupffer's vesicle are required for specification of the zebrafish left-right axis. *Dev Biol* 287, 274-88 (2005).
5. Amack, J. D., Wang, X. & Yost, H. J. Two T-box genes play independent and cooperative roles to regulate morphogenesis of ciliated Kupffer's vesicle in zebrafish. *Dev Biol* 310, 196-210 (2007).
6. Kane, D. A., McFarland, K. N. & Warga, R. M. Mutations in half baked/E-cadherin block cell behaviors that are necessary for teleost epiboly. *Development* 132, 1105-16 (2005).
7. Esguerra, C. V. et al. Ttrap is an essential modulator of Smad3-dependent Nodal signaling during zebrafish gastrulation and left-right axis determination. *Development* 134, 4381-93 (2007).
8. Matsui, T. et al. Noncanonical Wnt signaling regulates midline convergence of organ primordia during zebrafish development. *Genes Dev* 19, 164-75 (2005).
9. Amack, J. D. & Yost, H. J. The T box transcription factor no tail in ciliated cells controls zebrafish left-right asymmetry. *Curr Biol* 14, 685-90 (2004).
10. Neugebauer, J. M., Amack, J. D., Peterson, A. G., Bisgrove, B. W. & Yost, H. J. FGF signalling during embryo development regulates cilia length in diverse epithelia. *Nature* 458, 651-4 (2009).
11. Ito, Y., Matsui, T., Kamiya, A., Kinoshita, T. & Miyajima, A. Retroviral gene transfer of signaling molecules into murine fetal hepatocytes defines distinct roles for the STAT3 and ras pathways during hepatic development. *Hepatology* 32, 1370-6 (2000).

12. Shimizu, T. et al. E-cadherin is required for gastrulation cell movements in zebrafish. *Mech Dev* 122, 747-63 (2005).
13. Pownall, M. E. et al. An inducible system for the study of FGF signalling in early amphibian development. *Dev Biol* 256, 89-99 (2003).